



1 Denitrification in soil as a function of oxygen supply and demand at 2 the microscale

3 Lena Rohe¹, Bernd Apelt¹, Hans-Jörg Vogel¹, Reinhard Well², Gi-Mick Wu³, Steffen Schlüter¹

4 ¹Helmholtz Centre for Environmental Research – UFZ, Department Soil System Sciences, Theodor-Lieser-5 Str. 4,
5 06120 Halle, Germany

6 ²Thünen Institute of Climate Smart Agriculture, Bundesallee 65, 38116 Braunschweig, Germany

7 ³Helmholtz Centre for Environmental Research – UFZ, PACE, Permoserstraße 15, 04318 Leipzig, Germany

8 *Correspondence to:* Lena Rohe, (lena.rohe@ufz.de)

9 **Abstract**

10 The prediction of nitrous oxide (N₂O) and of dinitrogen (N₂) emissions formed by biotic denitrification in
11 soil is notoriously difficult, due to challenges in capturing co-occurring processes at microscopic scales.
12 N₂O production and reduction depend on the spatial extent of anoxic conditions in soil, which in turn are
13 a function of oxygen (O₂) supply through diffusion and O₂ demand by respiration in the presence of an
14 alternative electron acceptor (e.g. nitrate).

15 This study aimed to explore controlling factors of complete denitrification in terms of N₂O and (N₂O+N₂)
16 fluxes in repacked soils by taking micro-environmental conditions directly into account. This was
17 achieved by measuring micro-scale oxygen saturation and estimating the anaerobic soil volume fraction
18 (*ansvf*) based on internal air distribution measured with X-ray computed tomography (X-ray CT). O₂
19 supply and demand was explored systemically in a full factorial design with soil organic matter (SOM,
20 1.2 and 4.5%), aggregate size (2-4 and 4-8mm) and water saturation (70, 83 and 95% WHC) as factors.
21 CO₂ and N₂O emissions were monitored with gas chromatography. The ¹⁵N gas flux method was used to
22 estimate the N₂O reduction to N₂.

23 N-gas emissions could only be predicted well, when explanatory variables for O₂ supply and oxygen
24 demand were considered jointly. Combining *ansvf* and CO₂ emission as proxies of O₂ supply and demand
25 resulted in 83% explained variability in (N₂O+N₂) emissions and together with the denitrification product
26 ratio [N₂O/(N₂O+N₂)] (*pr*) 72% in N₂O emissions. O₂ concentration measured by microsensors was a
27 poor predictor due to the variability in O₂ over small distances combined with the small measurement
28 volume of the microsensors. The substitution of predictors by independent, readily available proxies for
29 O₂ supply (diffusivity) and O₂ demand (SOM) reduced the predictive power considerably (50% and 58%
30 for N₂O and (N₂O+N₂) fluxes, respectively).



31 The new approach of using X-ray CT imaging analysis to directly quantify soil structure in terms of *ansvf*
32 in combination with N₂O and (N₂O+N₂) flux measurements opens up new perspectives to estimate
33 complete denitrification in soil. This will also contribute to improving N₂O flux models and can help to
34 develop mitigation strategies for N₂O fluxes and improve N use efficiency.

35

36 Keywords: anaerobic soil volume fraction, air distance, diffusivity, nitrous oxide, dinitrogen, oxygen
37 microsensors, product ratio, X-Ray computed tomography (X-ray CT)

38 **1. Introduction**

39 Predicting emissions of the greenhouse gas nitrous oxide (N₂O) is important in order to develop
40 mitigation strategies. Agriculture accounts for approximately 60% of anthropogenic N₂O emissions, most
41 likely because high amounts of substrates for N₂O producing processes result from nitrogen (N)
42 fertilization on agricultural fields (Syakila and Kroeze, 2011; Thompson et al., 2019). The required
43 process understanding is hindered, since various microbial species are capable of N₂O production via
44 several pathways and these may co-exist due to different micro-environmental conditions within short
45 distances in soil (Hayatsu et al., 2008; Braker and Conrad, 2011). Denitrification is one of the major
46 biological pathways for N₂O production, which describes the reduction of nitrate (NO₃⁻) as the alternative
47 electron acceptor into the trace gas nitrous oxide (N₂O) as an intermediate and molecular nitrogen (N₂) as
48 the final product (Knowles, 1982; Philippot et al., 2007). Although it is well known that not all microbial
49 species are capable of denitrification pathway, it is particularly widespread among bacteria, but also
50 several fungi and even archaea can denitrify (Shoun et al., 1992; Cabello et al., 2004).

51 N₂O emissions from soils are often considered to be erratic in nature due to their high variability in space
52 and time (Butterbach-Bahl et al., 2013). The low predictability is caused by the mechanisms that regulate
53 microbial denitrification at the pore scale which are concealed from measurement techniques that average
54 across larger soil volumes. This experimental study is designed to reveal the drivers of oxygen (O₂)
55 supply and demand at the microscale that govern microbial denitrification at the macroscale.

56 In general, there are several controlling factors for microbial denitrification in soil. Proximal factors,
57 such as N and carbon (C) are needed to ensure the presence of electron acceptors and electron supply. In
58 addition, the absence of oxygen is required to express the enzymes for the reduction of reactive nitrogen.
59 Distal factors, i.e. physical and biological factors like soil structure, soil texture, pH or microbial
60 community, on the other hand affect the proximal factors (Groffman and Tiedje, 1988; Tiedje, 1988). The
61 main physical controlling factors that regulate O₂ supply are water saturation and soil structure, because
62 they determine the pathways through which gaseous and dissolved oxygen, but also NO₃⁻ and dissolved



63 organic matter may diffuse towards the location of their consumption. Likewise they determine the
64 pathways through which denitrification products may diffuse away from these locations. In addition, both,
65 saturation and soil structure, contribute to the regulation of O₂ demand through their impact on substrate
66 accessibility and thus microbial activity (Keiluweit et al., 2016). Studies have shown microbial activity,
67 described by microbial respiration, to increase with increasing water saturation, but it also decreased
68 when water saturation exceeded a certain optimal value at intermediate conditions (Davidson et al., 2000;
69 Reichstein and Beer, 2008; Moyano et al., 2012). Low water saturation causes C substrate limitations
70 whereas high water saturation causes limited oxygen diffusion (Davidson et al., 2000). This observation
71 goes along with an increase of anaerobic respiration in microbial hot spots when O₂ demand exceeded O₂
72 supply and denitrification is favoured (Balaine et al., 2015).

73 These physical processes that govern denitrification at the microscale have to be effectively described
74 by macroscopic bulk soil properties in order to improve the predictability of denitrification activity at
75 larger scales. It has been shown repeatedly that soil diffusivity can be used to predict the impact of O₂
76 supply on N₂O and N₂ emissions (Balaine et al., 2016; Andersen and Petersen, 2009). First N₂O emissions
77 increase with decreasing diffusivity, but then it dramatically decreases due to N₂ production when
78 diffusivity is extremely low.

79 Diffusivity is not routinely measured in denitrification studies as it is more difficult to measure than air
80 content or water saturation, but there are many empirical models to estimate diffusivity based on air filled
81 pore volume (Millington and Quirk, 1961; Moldrup et al., 1999; Deepagoda et al., 2011; Millington and
82 Quirk, 1960). All of these metrics are only indirect metrics of the anaerobic soil volume fraction (*ansvf*)
83 as direct measurements are difficult to obtain. Either it is measured locally via oxygen sensors with
84 needle-type microsensors (Sexstone et al., 1985; Højberg et al., 1994; Elberling et al., 2011) or with foils
85 (Keiluweit et al., 2018; Elberling et al., 2011), which requires to average or to extrapolate measured O₂
86 saturation for the entire soil volume. Or it is estimated for the entire sample volume from pore distances
87 in X-ray CT images of soil structure assuming that there is a direct relationship between pore distances
88 and anaerobiosis (Kravchenko et al., 2018; Rabot et al., 2015).

89 Completeness of denitrification is another important controlling factor that modulates the relationship
90 between oxygen availability and N₂O emissions (Morley et al., 2014) which has previously been
91 neglected in similar incubation studies (Rabot et al., 2015; Porre et al., 2016; Kravchenko et al., 2018)
92 due to methodological challenges imposed by measuring N₂ emissions from soil (Groffman et al., 2006).
93 Complete denitrification generates N₂ as the final product although it is assumed that 30% of denitrifying
94 organisms lack the N₂O reductase (Zumft, 1997; Braker and Conrad, 2011; Jones et al., 2008). Thus the
95 denitrification product ratio [N₂O/(N₂O+N₂)] (*pr*) was found to be very variable in soil studies covering
96 the whole range between 0 and 1 (Senbayram et al., 2012; Buchen et al., 2016). Decreasing *pr*, i.e.



97 relative increasing N_2 fraction compared to that of N_2O , were found with lower oxygen availability in
98 consequence of higher water saturations and denitrification activities in soil (van Cleemput, 1998).
99 In this paper, we will reconcile all these metrics, i. e. soil structure, bulk respiration, diffusivity, O_2
100 distribution, *ansvf* and *pr* to assess their suitability to predict denitrification activity. This requires well
101 defined laboratory experiments that either control or directly measure important distal controlling factors
102 of denitrification activity like microbial activity, anaerobic soil volume and denitrification completeness.
103 To this end the current study presents a comprehensive experimental setup with well-defined
104 experimental conditions but also micro-scale measurements of oxygen concentrations, soil structure and
105 the air and water distribution at the pore scale. The ^{15}N tracer application was used to estimate the N_2O
106 reduction to N_2 and the N_2O fraction originating from denitrification. To our knowledge this is the first
107 experimental setup analyzing N_2O and (N_2O+N_2) fluxes in combination with X-ray CT derived structure.
108 Other important factors controlling denitrification like temperature, pH, nitrate limitation or plant-soil
109 interactions were either controlled or excluded in this study.

110 The general objective of the present study is to systematically explore bulk respiration and denitrification
111 as a function of O_2 supply and demand in repacked soils under static hydraulic conditions. O_2 demand
112 was controlled by incubating soils with different soil organic matter (SOM) content. O_2 supply was
113 controlled by different water saturations and different aggregate sizes. A novel approach is explored to
114 assess microscopic O_2 supply directly from *ansvf* estimates based on the distribution and continuity of air-
115 filled pores within the wet soil matrix.

116 We hypothesize that the combination of at least one proxy for O_2 supply (e.g. *ansvf*, diffusivity, air
117 content) and one for O_2 demand (CO_2 production) is required to predict complete denitrification
118 (N_2O+N_2), whereas *pr* as a proxy for denitrification completeness is required in addition to predict a
119 single component (N_2O)., The specific aims of our study were a) to investigate the potential of
120 microscopic metrics for O_2 supply such as *ansvf* to predict complete denitrification activity and b) to
121 explore as to how far a substitution of these predictors by classical, averaged soil properties required for
122 larger scale denitrification models is acceptable.

123 **2. Materials and Methods**

124 **2.1 Incubation**

125 Fine-textured topsoil material was collected from two different agricultural sites in Germany
126 (Rotthalmünster (RM) and Gießen (GI), (Table 1). These soils were chosen for the contrast in properties
127 potentially affecting denitrification and respiration (SOM contents, pH, texture, bulk density) which



128 induces a large difference in microbial respiration and hence O₂ demand under identical incubation
129 settings. The soils were sieved (10 mm), air-dried and stored at 6°C for several months before sieving into
130 two different aggregate size fractions: small (2-4 mm) and large (4-8mm). Care was taken to remove free
131 particulate organic matter like plant residues and root fragments during sieving. Other aggregate size
132 classes were not considered, as sieving yielded in a too low amount of larger aggregates that contained
133 too much irremovable POM, whereas smaller aggregate classes resulted in a too fragmented pore space at
134 the chosen scan settings.

135 **Table 1: Basic description of soil materials used for incubation (SOM – soil organic matter).**

Site	Landuse	Soil type (WRB)	Bulk density [g/cm ³]	Clay [%]	Silt [%]	SOM [%]	C:N	pH (CaCl ₂)
Rotthalmünster (RM)	arable	Luvisol	1.3	19	71	1.21	8.7	6.7
Gießen (GI)	grassland	Gleysol	1.0	32	41	4.46	10.0	5.7

136

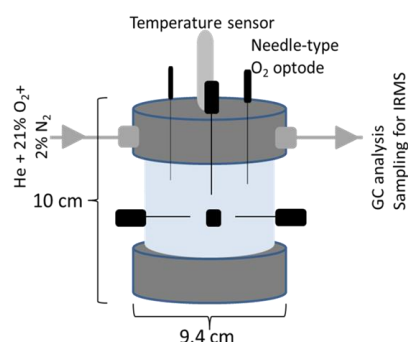
137 The soil material was pre-incubated at 50% water holding capacity (WHC) for two weeks to induce
138 microbial activity after the long dry spell and let the flush in carbon mineralization pass that occurs after
139 rewetting the soil. ¹⁵N labeled NO₃⁻ solution was applied when adjusting WHC to 70% before packing by
140 mixing 99 at% ¹⁵N-KNO₃ (Cambridge Isotope Laboratories, Inc., Andover, MA, USA) and unlabelled
141 KNO₃ (Merck, Darmstadt, Germany) to reach 50 mg N kg⁻¹ soil and 60 atom%. This ¹⁵N-labelled soil was
142 filled into cylindrical PVC columns (9.4cm inner diameter x10cm height) (Figure 1) and compacted to a
143 target bulk density that correspond to site-specific topsoil bulk densities (Jäger et al., 2003; John et al.,
144 2005). The incubation of such repacked soils instead of intact soil columns was chosen to i)
145 systematically investigate the effect of aggregate size and to ii) guarantee thorough mixing of the ¹⁵N
146 tracer with the soil.

147 Packing in five vertical intervals achieved a uniform porosity across the column. However, there were
148 inevitable porosity gradients within intervals (Figure S4) that affected the air and water distribution and
149 thus air continuity at high water saturations. Three different saturation treatments were prepared for
150 subsequent incubation experiments: 70%, 83% and 95% WHC. For the latter two saturation levels
151 additional NO₃⁻ solution was sprayed sequentially onto each layer after packing. In this way, a full
152 factorial design with twelve treatments and three factors (soil: RM, GI; aggregate size: large, small;
153 saturation: 70, 83, 95 % WHC) were prepared in triplicates for incubation. WHC was additionally
154 measured for both soil materials in parallel soil cores. For a better comparability with previous studies the
155 results will be presented in terms of water-filled pore space (WFPS), which is derived from the known



156 mass of soil and water and their respective densities. A detailed description of the experimental setup can
157 be found in the Supplementary Material.

158



159

160 **Figure 1: Schematic of the column for repacked soil showing the dimension (10x9.4 cm), the lid with in- and outlet**
161 **for technical gas (21% O₂ and 2 % N₂ in helium), in black O₂ microsensors and in gray the temperature sensor located in**
162 **soil core.**

163

164 The columns containing the packed soil aggregates were closed tightly and were equipped with an in-
165 and outlet in the headspace (Figure 1). To analyse O₂ saturation, needle-type (40x0.8mm) oxygen
166 microsensors with <140µm flat-broken sensor tip (NFSG-PSt1, PreSens Precision Sensing GmbH,
167 Regensburg, Germany) were pinched through sealed holes in the lid and PVC column at seven well
168 defined positions. Three sensors were located at the top by inserting vertically into the soil through the lid
169 and headspace down to approximately 20mm depth, whereas four sensors were inserted laterally at the
170 centre of the column in about 36mm depth with angular intervals of 90°. The microsensors were coupled
171 to a multi-channel oxygen meter (OXY-10 micro, PreSens Precision Sensing GmbH, Regensburg,
172 Germany) and O₂ measurements were stored in 15min intervals. The O₂ data were aggregated to 6 hour
173 means for further analysis. The columns were placed in a darkened, temperature-controlled 20°C water
174 bath (JULABO GmbH, Seelbach, Germany). Two flow controllers (G040, Brooks® Instrument, Dresden,
175 Germany) served to flush the columns with technical gas (21% O₂ and 2% N₂ in helium, Praxair,
176 Düsseldorf, Germany) through the inlet of the columns at a rate of 5ml min⁻¹. Initially, the headspace was
177 flushed with technical gas for approximately 3 to 5 hours under 6 cycles of mild vacuum (max. 300mbar)
178 to bring down the N₂ concentration within the soil column approximately to that of the technical gas (2%)
179 and to ensure comparable initial conditions for incubation. Incubation time was 192 hours. Additional
180 information on a parallel incubation where atmospheric conditions were switched from oxic to anoxic
181 conditions to calculate the anaerobic soil volume fraction ($ansvf_{cal}$) can be found in the Supplementary
182 Material.



183 2.2 Gas analysis

184 Gas chromatography (GC)

185 The columns outlet was directly connected to a gas chromatograph (Shimadzu 14B) equipped with an
186 electron capture detector (ECD) to analyse N₂O and two flame ionization detectors (FID) to analyse
187 methane (not reported) and CO₂. GC measurements were taken on-line every 6.5 minutes using GC
188 Solution Software (Shimadzu, GCSolution 2.40). The detection limit was 0.25ppm N₂O and 261.90ppm
189 CO₂ with a precision of at least 2 and 1%, respectively. The N₂O and CO₂ data were aggregated to 6 hour
190 means for further analysis in order to eliminate the high frequency noise from the otherwise gradually
191 changing gas concentrations under static incubation conditions. The measurements during an equilibration
192 phase of 24h were excluded. N₂O fluxes derived from GC analysis may include N₂O from other processes
193 than denitrification and is thus referred as the total net N₂O fluxes (*N₂O_{total}*).

194

195 Isotopic analysis

196 Samples for isotopic analysis of ¹⁵N in N₂O and N₂ were taken manually after 1, 2, 4, and 8 days of
197 incubation in 12 ml exetainers (Labco ©Exetainer, Labco Limited, Lampeter, UK). To elute residual air
198 from the 12 ml exetainer it was flushed three times with helium (helium 6.0, Praxair, Düsseldorf,
199 Germany) prior evacuating the air to 180 mbar. The exetainers were flushed with headspace gas for
200 15min, which amounts to a six-fold gas exchange of the exetainer volume. At the end of the incubation,
201 technical gas was also sampled to analyze the isotopic signature of the carrier gas.

202 These gas samples were analysed using an automated gas preparation and introduction system (GasBench
203 II, Thermo Fisher Scientific, Bremen, Germany, modified according to Lewicka-Szczebak et al. (2013)
204 coupled to an isotope ratio mass spectrometer (MAT 253, Thermo Fisher Scientific, Bremen, Germany)
205 that measured *m/z* 28 (¹⁴N¹⁴N), 29 (¹⁴N¹⁵N), and 30 (¹⁵N¹⁵N) of N₂ and simultaneously isotope ratios of
206 ²⁹R (²⁹N₂/²⁸N₂) and ³⁰R (³⁰N₂/²⁸N₂). All three gas species (N₂O, (N₂O+N₂), and N₂) were analysed as N₂
207 gas after N₂O reduction in a Cu oven. Details of measurement and calculations for fractions of different
208 pools (i. e. N in N₂O (*f_{p-N₂O}*) or N₂ (*f_{p-N₂}*) originating from ¹⁵N-labelled NO₃⁻ pool) were described
209 elsewhere and are provided in Supplementary Material (Supplementary Material, Figure S3) (Lewicka-
210 Szczebak et al., 2013; Spott et al., 2006; Buchen et al., 2016).

211 The product ratio (*pr*) [N₂O/(N₂O+N₂)] was calculated for each sample:

$$212 \quad pr [-] = \frac{f_{p-N_2O}}{f_{p-N_2O} + f_{p-N_2}} \quad (1)$$

213 The calculated average *pr* [N₂O/(N₂O+N₂)] of each treatment was also used to calculate the average total
214 denitrification fluxes (N₂O+ N₂ fluxes) during the incubation:

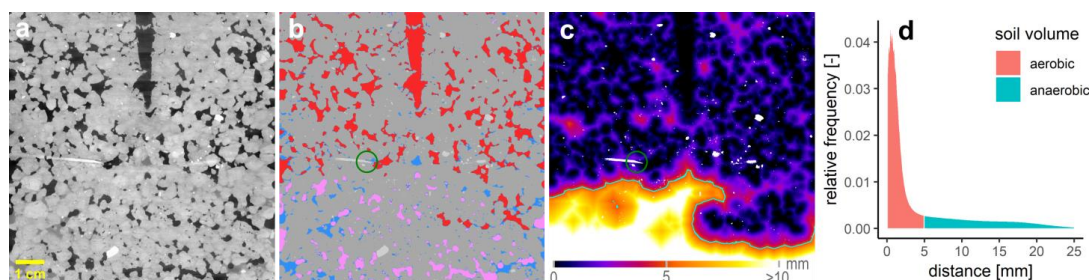
$$215 \quad (N_2O + N_2) [\mu g N h^{-1} kg^{-1}] = \frac{N_2O_{total}}{pr} \quad (2)$$



216 **2.3 Microstructure analysis**

217 Directly after the incubation experiment the soil cores were scanned with X-ray CT (X-tek XTH 225,
218 Nikon Metrology). The temperature sensor was removed, but the oxygen micro-sensors remained in place
219 during scanning. The scan settings (190 kV, 330 μ A, 708 ms exposure time, 1.5mm Cu filter, 2800
220 projections, 2 frames per projection) were kept constant for all soils and saturations. The projections were
221 reconstructed into a 3D tomogram with 8-bit precision and a spatial resolution of 60 μ m using the filtered
222 back projection algorithm in X-tek CT-Pro. Only macropores twice this nominal resolution were clearly
223 detectable in the soil core images. Hence, at the lowest water saturation not all air-filled pores can be
224 resolved, which will be discussed below. The 3D images were processed with the Fiji bundle for ImageJ
225 (Schindelin et al., 2012) and associated plugins. The raw data were filtered with a 2D non-local means
226 filter for noise removal. A radial and vertical drift in grayscale intensities had to be removed (Jassonov
227 and Tuller, 2010; Schlüter et al., 2016) before these corrected gray-scale images (Figure 2a) were
228 segmented into multiple material classes using the histogram-based thresholding methods (Schlüter et al.,
229 2014). The number of materials varied between two (air-filled pores, soil matrix) and four (air-filled
230 pores, water-filled pores, soil matrix, mineral grains) depending on saturation and soil material. By means
231 of Connected Components Labeling implemented in the MorpholibJ plugin (Legland et al., 2016) the air-
232 filled pore space was further segmented into isolated and connected air-filled porosity, depending on
233 whether there was a continuous path to the headspace (Figure 2b). Average oxygen supply in the core was
234 estimated by three metrics: 1) Visible air-filled porosity (ϵ_{vis}) and connected air content (ϵ_{con}) determined
235 by voxel counting (Figure2b), 2) average air distance derived from the histogram of the Euclidean
236 distances between all non-air voxels and their closest connected air voxel (Figure2c,d) (Schlüter et al.,
237 2019) and 3) the *ansvf* which corresponds to the volume fraction of air distance larger than a certain
238 threshold. Therefore, in a sensitivity test, air distance thresholds of 0.6, 1.3, 2.5, 3.8 and 5.0mm were used
239 to estimate the *ansvf* and to find the best correlation between *ansvf* and N_2O as well as (N_2O+N_2) fluxes.
240 This was found with an *ansvf* at a critical air distance of 5mm when pooling GI and RM soils
241 (Figure2c,d).

242 In summary, the ϵ_{con} is a proxy for the supply with gaseous oxygen coming from the headspace,
243 whereas the connected air distance and *ansvf* are proxies for the supply limitation of dissolved oxygen by
244 diffusive flux through the wet soil matrix. In addition to these averages for entire soil cores, both ϵ_{con} and
245 average air distance were also computed locally in the vicinity of oxygen sensor tips (Figure 2b-c), to
246 compare these metrics with measured oxygen concentrations. Spherical regions of interest (ROI) with
247 different diameters from 3.6 to 10.8mm were tested with respect to highest correlation of ϵ_{con} and average
248 air distance with average oxygen concentration of individual sensors. This was found to occur at a
249 diameter of 7.2mm, when centered on the sensor tip.



250
251
252
253
254
255
256
257

Figure 2: (a) 2D slice of packed GI soil with large aggregates and 75% WFPS. One oxygen microsensor is shown on the left and the hole of the temperature sensor at the top. (b) Material classes including soil matrix (gray), water (blue), mineral grains (light gray), connected air (red) and isolated air (rose). The green circle around the sensor tip depicts the diameter of 7.2mm that is used to characterize its environment. (c) Euclidean distance to the closest connected air voxels (mineral grains are excluded). The green line depicts the connected air distance threshold of 5mm that differentiates between an anaerobic soil volume fraction (light colors) or aerated volume. (d) Relative frequency of soil volume as a function of distance to closest connected air [mm] divided into aerobic (red) and anaerobic (green).

258

259 In addition to scans of the entire core, four individual aggregates (4-8mm) of each soil were also
260 scanned with X-ray CT (80 kv, 75 μ A, 1s exposure time, no filter, 2400 projections, 2 frames per
261 projection), reconstructed in 8-bit at a voxel resolution of 5 μ m, filtered with a 2D non-local means filter
262 and segmented into pores and background with the Otsu thresholding method (Otsu, 1975). The largest
263 cuboid fully inscribed in an aggregate was cut and used for subsequent diffusion modelling as described
264 below.

265 **2.4 Diffusivity simulations**

266 Diffusivity was simulated for individual aggregates as well as for the entire soil core (bulk diffusivity)
267 directly on segmented X-ray CT data by solving the Laplace equation with the DiffuDict module in the
268 GeoDict 2019 Software (Math2Market GmbH, Kaiserslautern, Germany). A hierarchical approach was
269 used to (1) estimate the effective diffusivity of the wet soil matrix by simulating Laplace diffusion on
270 individual soil aggregates with the Explicit Jump solver (Wiegmann and Zemitis, 2006; Wiegmann and
271 Bube, 2000) and (2) model diffusivity (D_{sim}) with the Explicit Jump solver on the entire soil core
272 (1550x1550x[1500-1600] voxels). The latter was based on the visible 3D pore space and using the
273 effective diffusion coefficient of the soil matrix as obtained from the simulation of soil aggregates. We
274 assumed an impermeable exterior, impermeable mineral grains (GI only) and the diffusion coefficient of
275 oxygen in air and water ($\geq 75\%$ WFPS only) in the respective material classes (see detailed information in
276 Supplementary Material).

277

278



279 **2.5 Statistical analysis**

280 Statistical analysis was conducted with R (R Core Team, 2018). Figures were produced with package
281 ggplot2 (Wickham, 2016). In order to estimate the correlation between various variables that do not
282 exhibit a normal distribution (average values of N₂O fluxes, (N₂O+N₂) fluxes, CO₂ fluxes, O₂ saturation,
283 *D_{sim}*, *ε_{con}*, *ansvf* and *pr*) Spearman's rank correlations with pairwise deletion of missing values was
284 performed pooling data for GI and RM soils. The p-values were corrected for multiple comparison
285 according to Benjamini and Hochberg (1995) and adjusted p-values ≤ 0.05 were considered as significant.

286 As described before, there were four missing values for *pr* due to limitation of the isotopic
287 measurement at the lowest saturation. For further statistical analysis of the dataset, any missing *pr* values
288 were imputed using the chained random forest using more than 100 regression trees, in terms of overall
289 variable pattern, as this method can handle nonlinear relationships between variables (Breiman, 2001;
290 Nengsih et al., 2019). It was also required to standardize the data of very different value ranges for further
291 analysis. Since N₂O and/or (N₂O+N₂) were not detectable for a few samples at the lowest saturation, a
292 constant of 1 was added to N₂O and (N₂O+N₂) fluxes prior transformation. This changes the mean value
293 but not the variance of data. In order to get normal distributions and linear relationships, a logarithmic
294 transformation was applied to metric data (CO₂, N₂O and (N₂O+N₂) fluxes, *D_{sim}*), whereas a logistic
295 transform $\text{logit}(x) = \log(x/(1 - x))$ was applied to dimensionless ratios between 0 and 1 (*ansvf*).

296 Since there was a high collinearity among most variables, a partial least square regression (PLSR)
297 with Leave-One-Out Cross-validated R² was the best method to identify the most important independent
298 explanatory variables (six predictors: CO₂ fluxes, O₂ saturation, *D_{sim}*, *ε_{con}*, *ansvf* and *pr*) to predict the
299 response variables N₂O or (N₂O+N₂) fluxes. It has to be emphasized that N₂O fluxes and *pr* were
300 measured independently of each other using different measuring methods (gas chromatography and
301 isotopic analysis) what justifies *pr* as a predictor variable for N₂O fluxes. In contrast to this (N₂O+N₂)
302 fluxes were calculated from *pr* and therefore *pr* was not included in PLSR for the response variable
303 (N₂O+N₂) fluxes (resulting in five explanatory variables). Bootstrapping was used to provide confidence
304 intervals that are robust against deviations from normality (R package boot v. 1.3-24) (Davison and
305 Hinkley, 1997; Cauty and Ripley, 2019). Given the relatively small sample size (36 incubations in total),
306 the smoothed bootstrap was used by resampling from multivariate kernel density (R package kernelboot
307 v. 0.1.7) (Wolodzko, 2020). The BCa bootstrap confidence interval of 95% of R² was a measure to
308 explain the variability in each response variable (Efron, 1987). Components that best explained N₂O and
309 (N₂O+N₂) fluxes were identified by permutation testing.

310 To address the second research question of this study concerning substitutions of predictors by
311 classical, averaged soil properties additional and simplified models with the PLSR approach described



312 above were performed using various variables to substitute most important predictors for N₂O or
313 (N₂O+N₂) fluxes. A detailed description of the substitution is provided in the result section 3.4 and
314 discussion section 4.2.

315 **3 Results**

316 **3.1 Bulk respiration**

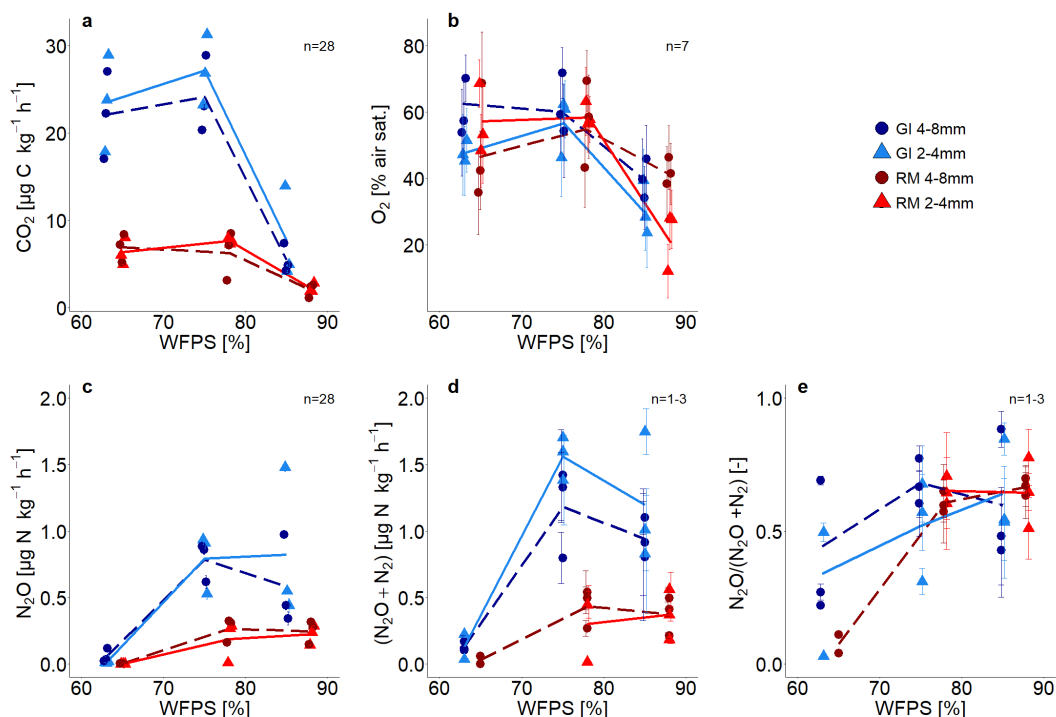
317 Time series of CO₂ and N₂O fluxes (Supplementary Material, Figure S1) show aggregated values for
318 six hour steps over the complete incubation time of approximately 192 hours, ignoring the first 24 hours
319 due to initial equilibration of the system. Averages for the whole incubation are reported in Figure 3a, 3c
320 and in Supplementary Material, Table S1, Table S2. The 3.7 times higher SOM content in GI soil than in
321 RM soil resulted in higher microbial activity so that CO₂ fluxes were approximately 3 times higher, for all
322 saturations. The variability in CO₂ fluxes between replicates is much higher than the temporal variability
323 during incubation. This is probably explained by small differences in packing of the columns that can
324 have large consequences for soil aeration. CO₂ production in both soils was lowest with highest water
325 saturation (Figure 3a) but were quite similar for both treatments with saturations <80% WFPS. Aggregate
326 size had a negligible effect on CO₂ production. Substantial N₂O and (N₂O+N₂) emissions were detected
327 for saturations ≥75% WFPS and were again approximately three times higher in SOM-rich GI soil than in
328 RM soil (Figure 3c, d). The variability between replicates is again higher than the temporal variability
329 (e.g. in Figure 3d and time series in Supplementary Material, Figure S1) and the effect of aggregate size is
330 inconsistent due to the large variability among replicates. Mineral N was not analyzed after the incubation
331 and therefore cumulative (N₂O+N₂) fluxes were used to estimate the N loss after 192h of incubation.
332 Considering the N addition of 50mg N kg⁻¹ as NO₃⁻ and an average natural NO₃⁻ background of 34 mg kg⁻¹
333 ¹ substantial N loss was observed for both soils at ≥75% WFPS. In RM soil the N converted to N₂O or N₂
334 represents a proportion equal to 2-4% for both aggregate sizes and saturations. With GI soil incubated at
335 75% WFPS the N loss was on average 5-11% for both aggregate sizes, whereas it reached 14% at 85%
336 WFPS.

337 Average O₂ saturation was lowest with highest water saturation and roughly the same for saturations
338 <80%WFPS (Figure 3b). Some sensors showed a gradual decline in O₂ concentration, whereas some
339 showed a drastic reduction or increase in a short period of time, probably due to water redistribution
340 (Supplementary Material, Figure S2). The average of the final 24h was taken for all subsequent analysis,
341 as this probably best reflects the water distribution scanned with X-ray CT. Standard errors among the



342 seven O₂ microsensors were high in each treatment due to very local measurement of O₂ that probed very
343 different locations in the heterogeneous pore structure.

344 The *pr*, i.e. the N₂O/(N₂O+N₂) as a measure of denitrification completeness, showed a similar behavior as
345 a function of water saturation like N₂O release with a plateau for saturations ≥75% WFPS at 0.6 and a
346 lower, but somewhat more erratic *pr* for the lowest saturation due to a generally low ¹⁵N gas release
347 (Figure 3e). Thus, the (N₂O+N₂) fluxes at ≤65% WFPS could only be calculated for a small number of
348 samples, due to lacking data of *pr* (Supplementary Material, Table S1, Table S4). SOM content and
349 aggregate size had no effect on *pr*. Time series of *pr* showed a gradual reduction for all treatments as the
350 N₂ emissions grew faster than the N₂O emissions (Supplementary Material, Figure S5). With water
351 saturations >75% WFPS the *pr* decreased with time and was in most cases <0.5 at the end of incubation
352 (Supplementary Material, Figure S5). In summary, for each soil all samples with saturation ≥75% WFPS
353 showed similar *pr* (Figure 3e) and N₂O release (Figure 3c). This agreed well with subsequent X-ray CT
354 estimates of air connectivity as shown below.



355

356 Figure 3: (a) Average CO_2 fluxes, (b) average O_2 saturation, (c) average N_2O and (d) $(\text{N}_2\text{O} + \text{N}_2)$ fluxes and (e) average
 357 product ratio (pr) $[\text{N}_2\text{O}/(\text{N}_2\text{O} + \text{N}_2)]$ as a function of water saturation for soil from Rothalmünster (RM) and Gießen (GI)
 358 and two aggregate sizes (2-4 and 4-8 mm). Symbols depict the average values for each of three individual replicates with
 359 error bars showing the standard error of the mean; standard error in (a) and (c) of fluxes measured during incubation, in
 360 (b) the standard error from measurements of seven sensors located within the soil core and in (d) and (e) of three
 361 measurements during incubation time (after 2, 4, and 8 days with detectable R^{29} and R^{30} ; $n = 3$ for two highest WFPS).
 362 The lines (dashed and solid) connect the average value of three replicates at each saturation (large and small aggregates,
 363 respectively).
 364

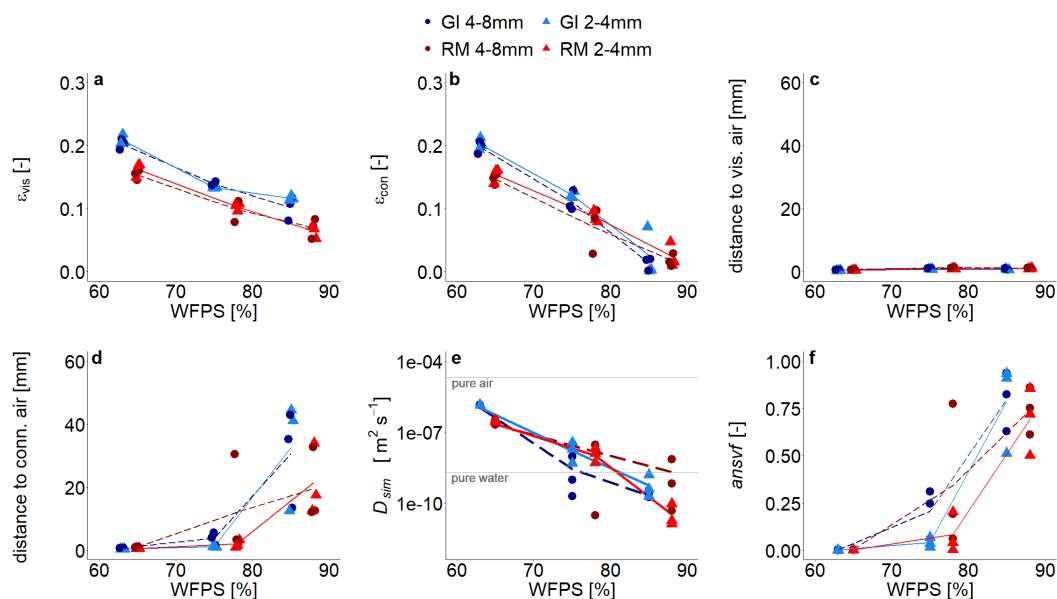
364

365 3.2 Pore system of soil cores

366 Due to lower target bulk density in GI soil (1.0 g cm^{-3}) compared to that of RM soil (1.3 g cm^{-3})
 367 visible air content (ϵ_{vis} , depicted in red and pink in Figure 2c) was higher independent of aggregate size
 368 (Figure 4a). The ϵ_{vis} decreased with increasing water saturation, but not linearly as would be expected.
 369 The air contents in the very wet range are in fact higher (16-17%), than the target air saturation of
 370 approximately 11 or 15% for RM and GI soil, respectively. It was not possible to remove air more
 371 efficiently during packing and some ponding water might have accidentally been removed with vacuum
 372 application during purging at the beginning of incubation. Additionally, the GI soil was rich in
 373 vermiculite and swelled upon wetting. This increase in soil volume at the end of incubation resulted in a
 374 relative decline in water content. For increasing water content the air content that is connected to the



375 headspace (ϵ_{con} , depicted in red in Figure 2c) was reduced much more strongly as compared to the total
 376 ϵ_{vis} . This was observed for both soils and aggregate sizes and indicates that, a substantial amount of air is
 377 trapped (Figure 4b). According to this observation, average distance to visible air was very small (Figure
 378 4c) and remained below 1.5mm even for the highest water saturation with generally smaller distances for
 379 smaller aggregates. Yet, the average distance to the pore system connected with headspace escalates in
 380 the wet range (Figure 4d) which results in an *ansvf* of 50-90% (Figure 4f). The huge variability among
 381 replicates comes from the fact that trapping by complete water blockage typically occurs in the slightly
 382 compacted upper part of a packing interval, but the specific interval where this happens varies among
 383 samples (Supplementary Material, Figure S4). The different aggregate sizes did not affect the distance to
 384 connected air as the long-range continuity of air is controlled by bottle-necks in the pore space and not by
 385 aggregate size.



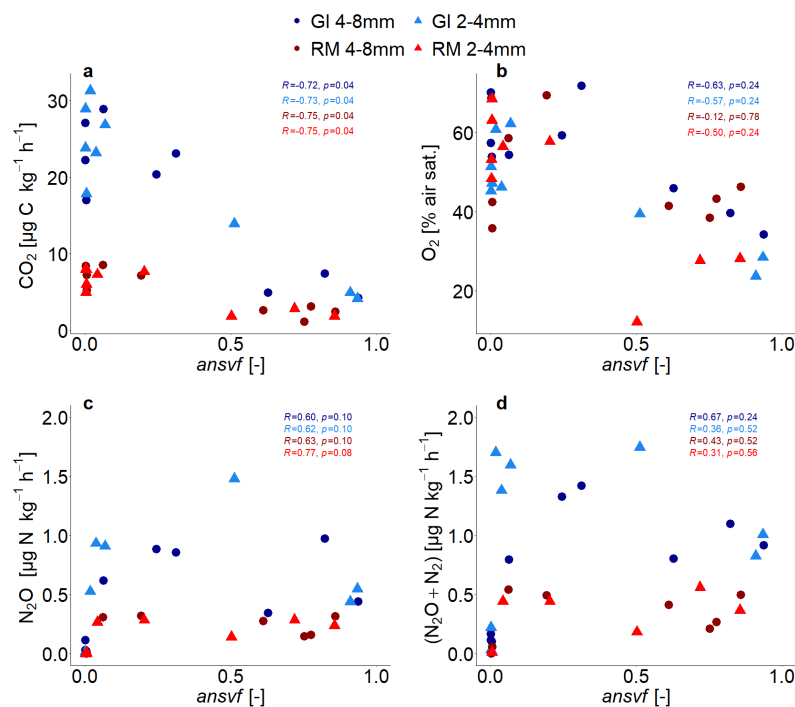
386
 387 **Figure 4:** (a) Visible air content (ϵ_{vis}), (b) connected air content (ϵ_{con}), (c) average distance to visible air, (d) average
 388 distance to connected visible air, (e) simulated diffusivity (D_{sim}) and (f) anaerobic soil volume fraction (*ansvf*) as a function
 389 of water saturation for soil from Rothalmünster (RM) and Gießen (GI), two aggregate sizes (2-4 and 4-8 mm) and three
 390 replicates each depicted by symbols. The lines (dashed and solid) connect the average value of three replicates (large and
 391 small aggregates, respectively). The horizontal gray lines in (e) reflect material properties. The experiment was performed
 392 at 20°C and according to that diffusivity was calculated at 20°C.

393

394 Water saturation had a dramatic impact on D_{sim} (Figure 4e) leading to a reduction by five orders of
 395 magnitude in a rather small saturation range. At high saturations it fell below the oxygen diffusion
 396 coefficient in pure water due to the tortuosity of the pore system.



397 The correlation of *ansvf* with average gas fluxes and internal O₂ concentrations is shown in Figure 5.
 398 Since the drop in CO₂ release at the highest water saturations coincided with an escalating *ansvf*, the
 399 relation between the two was highly correlated (Spearman's $R > -0.7$ and $p = 0.04$) for all soils and
 400 aggregate sizes (Figure 5a), but with different slopes for both soils due to vastly different SOM contents.
 401 The correlation of *ansvf* with N₂O is weaker (Spearman's $0.6 < R < 0.77$) and on the verge of being
 402 significant ($p \leq 0.1$) (Figure 5c). However, the correlation of *ansvf* with (N₂O+N₂) release is even worse
 403 ($p > 0.2$), so the mechanisms that govern N₂O and (N₂O+N₂) release must be more complex (Figure 5c, d).
 404 As expected the average O₂ saturation decreases with increasing *ansvf* (Figure 5b). Yet, correlation is
 405 lower than for CO₂ (Spearman's $-0.6 < R < -0.2$, but $p > 0.2$), likely due to limited representativeness of
 406 average O₂ concentrations derived from a few point measurements.



407
 408 **Figure 5: Average (a) CO₂ fluxes (b) O₂ saturation, (c) N₂O and (d) (N₂O+N₂) fluxes as a function of anaerobic soil**
 409 **volume fraction (*ansvf*) for soil from Rotthalmünster (RM) and Gießen (GI) and two aggregate sizes (2-4 and 4-8 mm) for**
 410 **three individual replicates. The Spearman's rank correlation coefficient (R) result from Spearman's rank correlation and**
 411 **indicate the extent of monotonic relation between the ranks of both variables. The associated p-values (p) were corrected**
 412 **for multiple comparison according to Benjamini and Hochberg (1995).**

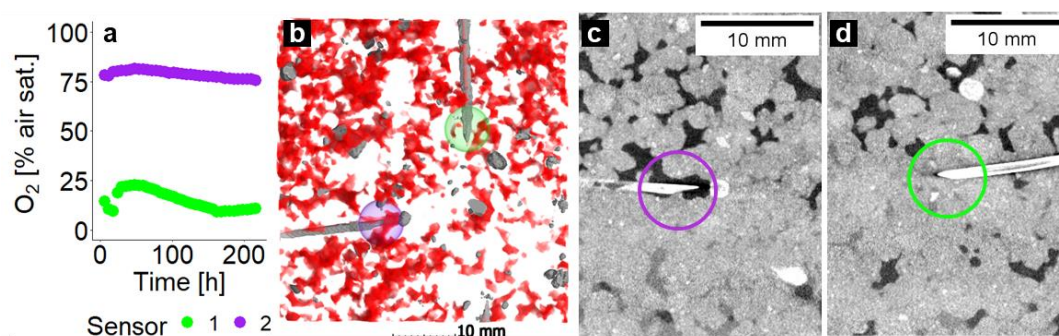
413

414 3.3 Microscopic oxygen distribution

415 The local measurements of O₂ using microsensors is demonstrated as an example for two selected
 416 sensors from the same soil column (GI soil incubated at 75% WFPS). They are located in the same depth



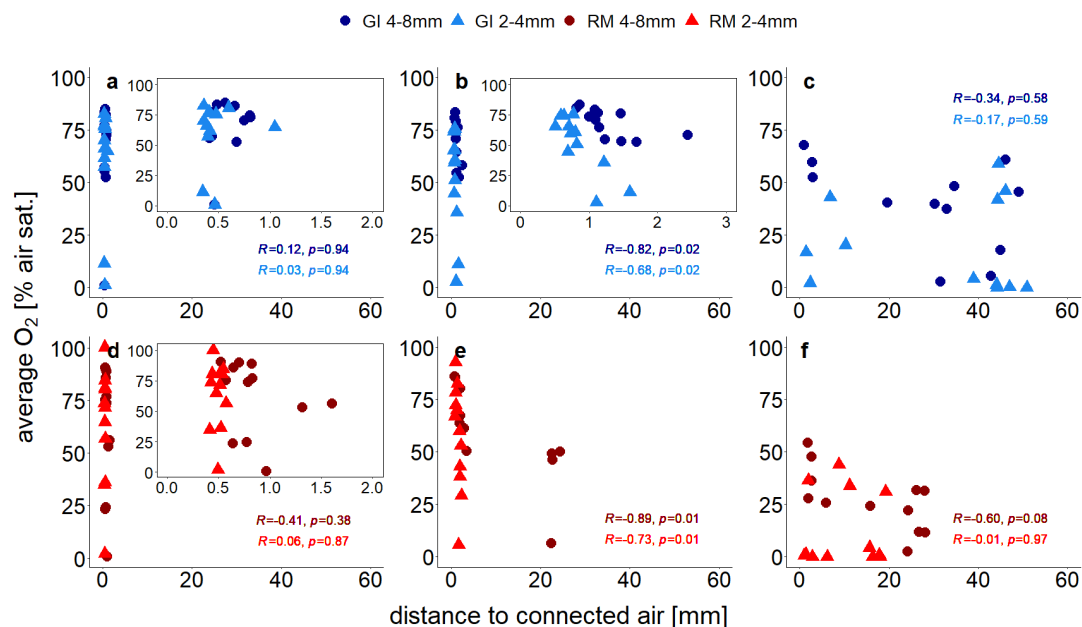
417 with a separation distance of $<2\text{cm}$. Sensor 1 detected low O_2 concentrations (18% air saturation) because
418 it was located in a compact area with low ϵ_{con} (4%) and a rather large distance to the closest air-filled pore
419 (1.6mm) (Figure 6a,b,d). Sensor 2 detected fairly high O_2 concentrations (76% air saturation) as it
420 happened to pinch into a macropore with a high ϵ_{con} (15%) and a short distance to connected air (0.8mm)
421 in its vicinity (Figure 6a-c). The green or violet circle with a diameter of 7.2mm depicts the spherical
422 averaging volume for ϵ_{con} and distance to connected air that correlated best with the average O_2
423 concentrations when lumped over all soils and saturations (Figure 6b-d).



424
425 **Figure 6:** Local oxygen distribution in one soil core packed with small aggregates (2-4mm) from Gießen soil (GI)
426 incubated at 75% WFPS to illustrate as an example the very local measurement of O_2 . Shown here are (a) O_2 saturations
427 measured by two microsensors as a function of incubation time, (b) a 3D subvolume showing both sensors (connected air
428 is depicted in red), and 2D images of the corresponding sensor tips (c) the sensor measuring high and (d) the sensor
429 measuring low O_2 saturations. The violet or green circles depict the proximity of the sensor tip (7.2 mm diameter) used to
430 calculate the averaged local metrics.

431 The treatment specific correlations between distance to connected air and average O_2 concentrations
432 are shown in Figure 7. At the lowest saturation level there is no correlation at all (Spearman's -
433 $0.4 << R < 0.1$ and $p \geq 0.38$, Figure 7a,d), because some unresolved pores ($<120\mu\text{m}$) within the aggregates
434 are air-filled so that oxygen availability is not limited by visible air. At the intermediate saturation level
435 the correlations were best (Spearman's $R < -0.7$ and $p \leq 0.02$) because all unresolved pores are water-filled
436 (Figure 7b,e). At the highest water saturation the correlation was highest for large aggregates (Spearman's
437 $R = -0.6$ and $p = 0.08$), because the local effect of soil structure might become stronger relative to the non-
438 local effect of air entrapment. With the other three treatments the correlation were worse again
439 (Spearman's R between -0.01 and -0.3 and $p \geq 0.58$, Figure 7c,f), because distance to connected air ignores
440 all trapped air which may still contribute a lot to oxygen supply.

441



442
 443 **Figure 7:** Average O₂ saturation (at the end of incubation experiment) measured with 4 sensors each located at the
 444 center of soil core as a function of distance to visible connected regression for soil from Rotthalmünster (RM, (a)-(c), red)
 445 and Gießen (GI, (d)-(f), blue), and for two aggregate sizes (2-4mm and 4-8mm). (a) and (d) show results for lowest (b) and
 446 (e) for medium and (c) and (f) for highest water saturation. The inset in (a), (b), and (d) shows a reduced distance range.
 447 The distance to visible connected air is averaged in a spherical region around the sensor tip (7.2 mm diameter). The
 448 Spearman's rank correlation coefficient (*R*) result from Spearman's rank correlation and indicate the extent of
 449 monotonic relation between the ranks of both variables. The associated p-values (*p*) were corrected for multiple
 450 comparison according to Benjamini and Hochberg (1995).

451

452 **3.4 Explanatory variables for denitrification**

453 So far the correlations among different explanatory variables and between explanatory variables and
 454 N-gas release have been shown for individual treatments, i.e. separately for each combination of soil and
 455 aggregate size, in order to focus on the effect of water saturation. However, the true potential of
 456 explanatory variables to predict denitrification can only be explored with the entire pooled data set, so
 457 that the variability in denitrification is captured more representatively.

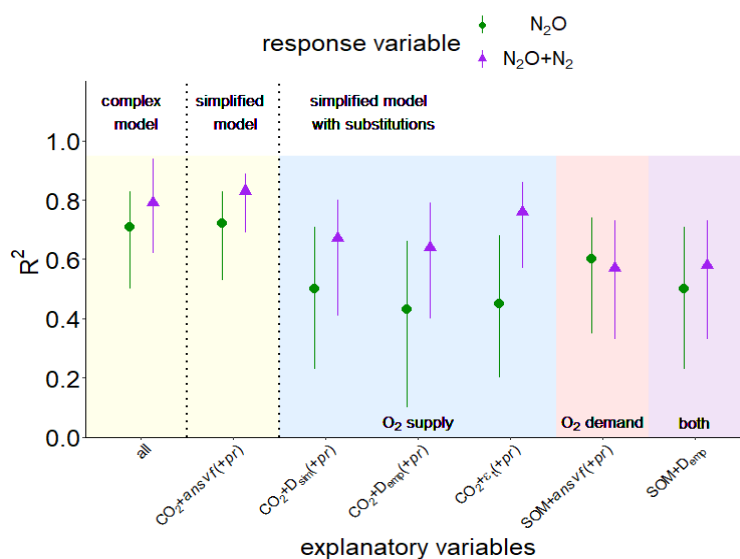
458 The PLSR identified two principal components that best explained N₂O and N₂O+N₂ fluxes, while
 459 most variables contributed to the first component (Comp1) and almost exclusively CO₂ release
 460 contributed to the second component (Comp2) (see Supplementary Material S7). These principal
 461 components revealed vastly different ability of individual explanatory variables to explain the observed
 462 variability in N₂O and (N₂O+N₂) release. The importance of explanatory variables to predict N₂O and
 463 N₂O+N₂ fluxes varied as follows: CO₂ > (*pr* >) *ansvf* > *D_{sim}* > *ε_{con}* > O₂ (see Supplementary Material
 464 Figure S7). Hereinafter *pr* shown in brackets illustrates its contribution to PLSR analysis for N₂O fluxes



465 only. The explanatory variability, expressed in the text as $R^2 \cdot 100$ [%], was 71% for N_2O fluxes and 79%
466 for N_2O+N_2 fluxes when considering the complex model with all explanatory variables (CO_2 flux, O_2
467 saturation, ε_{con} , D_{sim} , $ansvf$ (and pr)) (Figure 8). The resulting regression equations can be found in
468 Supplementary Material (Equation 3-6).

469 Starting from this complex model a series of simplifications and substitutions of explanatory variables
470 was conducted to assess in how far the resulting loss in predictive power is acceptable. Reducing the
471 number of explanatory variables to the most important variables resulted in CO_2 and $ansvf$ for (N_2O+N_2)
472 release (83% explained variability, simplified model in Figure 8). In other words, the combination of
473 these two predictors ($ansvf$ and CO_2) is crucial, as CO_2 release explains the different denitrification rates
474 between the two soils, whereas $ansvf$ explains the differences within a soil due to different saturations. To
475 predict N_2O emissions the simplified model with most important explanatory variables CO_2 , $ansvf$ and pr
476 as a third predictor resulted in 71% of explained variability (Figure 8). Average O_2 saturation could be
477 omitted for its small correlation with N_2O or (N_2O+N_2) release in general, whereas ε_{con} and D_{sim} could be
478 omitted because of the high correlation with $ansvf$ (Supplementary Material, Figure S6).

479 Various variables were used to substitute best predictors (CO_2 or $ansvf$) (Figure 8) in PLSR. The
480 substitution of CO_2 by SOM or $ansvf$ by ε_b , D_{sim} or empirical diffusivity (D_{emp}) based on total porosity and
481 air content (Deepagoda et al., 2011) is explained in the discussion section 4.2.



482
 483
 484
 485
 486
 487
 488
 489
 490
 491
 492
Figure 8: Explained variability expressed as R^2 with a confidence interval of 95% resulting from partial least square regression (PLSR) with Leave-One-Out Cross-validation and bootstrapping for response variables N_2O (green symbols) or (N_2O+N_2) fluxes (violet symbols) for pooled data of both soils (RM and GI), WFPS treatments and aggregate sizes ($n=36$). The yellow area shows a complex model including all explanatory variables of the present study (CO_2 , O_2 , connected air content (ϵ_{con}), diffusivity (D_{sim}), anaerobic soil volume fraction ($ansvf$), and product ratio (pr)) (all) and a simplified model included only most important predictors ($CO_2+ansvf(+pr)$). The blue area shows additional simplified models with substitutions of the most important predictor for O_2 supply ($ansvf$) by D_{sim} or diffusivity from calculated from an empirical model (D_{emp}) (Deepagoda et al., 2011), or theoretical air content (ϵ_i). The red area shows a simplified model with substitutions of the most important predictor for O_2 demand (CO_2) by SOM. Substitution of both most important predictors (CO_2 and $ansvf$) by SOM and D_{emp} is shown in the violet area.

493 **4 Discussion**

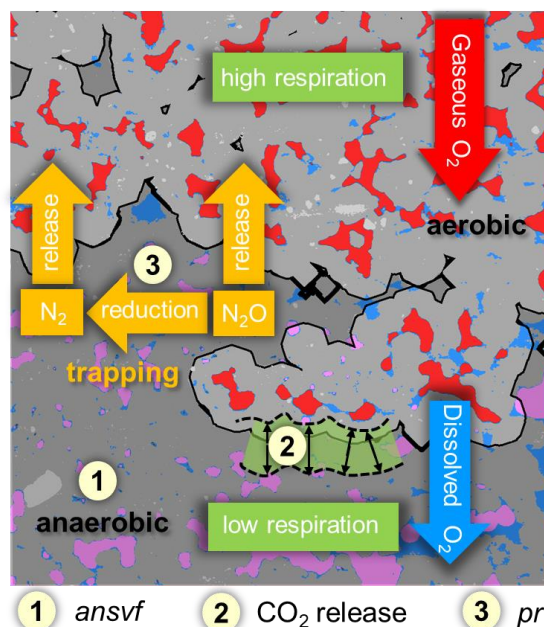
494 **4.1 Which processes govern denitrification in soil?**

495 The onset and magnitude of denitrification is controlled by O_2 supply and O_2 consumption, which in
 496 turn depends on processes in soil occurring at microscopic scales. This study was designed to examine
 497 different levels of O_2 consumptions by comparing soils with different SOM contents and different levels
 498 of O_2 supply by comparing different aggregate sizes and different water saturations. Other factors that
 499 would have affected O_2 demand (quality of organic matter, temperature, pH, plant-soil interactions), O_2
 500 supply (oxygen concentration in the headspace, temperature) or other drivers of denitrification (NO_3^-
 501 concentration, pH) were either controlled or excluded in this study.

502 N_2O release from soil can be low because denitrification does not occur under sufficient oxygen
 503 supply or because it is formed in wet soil but reduced to N_2 before it can escape to the atmosphere or
 504 because it is trapped in isolated air pockets (Braker and Conrad, 2011). Trapped N_2O is thought to likely



505 be reduced to N_2 eventually if gaseous N_2O is not released after a saturation change, which would open up
506 a continuous path to the headspace. This is shown in the schematic on the balance between O_2 supply and
507 demand and its effect on denitrification (Figure 9).
508



509
510 **Figure 9: Conceptual scheme of oxygen supply and demand and its effect on denitrification. Material classes including soil**
511 **matrix (gray area), water (blue), mineral grains (light gray), connected air (red) and isolated air (rose). The black line**
512 **divides between aerobic (light gray area) and anaerobic (dark gray area) conditions. Oxygen supply and demand regulate**
513 **the formation of anaerobic soil volume fraction (*ansvf*) as an imprint of the spatial distribution of connected air (item**
514 **number 1), respiration (item number 2) that would move the boundary between oxic and anoxic zones in the soil matrix**
515 **closer towards the pore when soil respiration is high (and vice versa) and N_2O reduction to N_2 (expressed by the product**
516 **ratio (*pr*), item number 3). The numbered items show how the explanatory variables that best describe N_2O release affect**
517 **denitrification.**

518
519 To our knowledge, the experimental setup of the present study combined for the first time
520 microstructure analysis of soil (X-ray CT) with measurements of N_2O and (N_2O+N_2) fluxes to explore
521 controlling factors of the complete denitrification process including N_2 formation. The explanatory
522 variables that contributed the highest predictive power with (N_2O+N_2) release were *ansvf* and CO_2 release
523 (Figure 9). The estimated *ansvf* (item 1) is a sole function of the spatial distribution of connected air in
524 soil and therefore only reflects soil structural properties related to O_2 supply. The dependence of
525 denitrification on diffusion constraints was demonstrated by several models that were developed to
526 predict the formation of anoxic centers within soil aggregates (Arah and Smith, 1989; Arah and Vinten,
527 1995; Greenwood, 1961; Kremen et al., 2005). The distance threshold for anoxic conditions to emerge
528 was set on an ad-hoc basis at 5mm from connected air, but is likely to vary with O_2 demand by local



529 microbial activity (CO₂ release represented by the green fringe area, item 2) (Kremen et al., 2005;
530 Keiluweit et al., 2018; Kravchenko et al., 2018; Schlüter et al., 2019; Ebrahimi and Or, 2018; Rabot et al.,
531 2015). In repacked soils it might be distributed rather uniformly and therefore correlated with bulk CO₂
532 release (Aon et al., 2001; Ryan and Law, 2005; Herbst et al., 2016). The fact that aggregate size had no
533 effect on denitrification indicates that critical distances were larger than the aggregate radii and rather
534 controlled by air distribution in the macropore system. This is in contrast to the very short critical
535 distances of 180µm for sufficient soil aeration estimated by Kravchenko et al. (2018) and Kravchenko et
536 al. (2019) for intact soil cores containing crop residues for which soil respiration was not determined but
537 likely to be much higher.

538 A somewhat surprising result is that oxygen concentration measurements did not have an added value
539 for predicting either N₂O release or total denitrification. Best correlation of local O₂ concentration with
540 ε_{con} was with a radial extent of 3.6mm used for averaging around the microsensor (Figure 7). Thus, with
541 seven microsensors per column we only probed 0.2% of the total soil volume. This is too small to capture
542 aerobic and anaerobic conditions representatively, especially since they may switch within short distances
543 (Figure 6). More sensors or sensors with larger support volume could be a means to improve the
544 predictive power of local oxygen measurements. However, there is always a trade-off between retrieving
545 more information and disturbing the soil is little as possible.

546 If only N₂O release is concerned, pr as an independent proxy for N₂O consumption (Figure 9 (item
547 3)) was beneficial to predict N₂O emissions together with CO₂ and $ansvf$ (Figure 8). The N₂O reduction to
548 N₂ and thus the pr are complexly controlled, where besides physical factors microbial (the structure of the
549 denitrifier community) and chemical properties (pH, N oxides, SOM, temperature, salinity) are relevant
550 (Müller and Clough, 2014; Clough et al., 2005; Smith et al., 2003). With respect to physical factors,
551 decreasing diffusivity enhances N₂O residence time and N₂O concentration in the pore space thus
552 favouring N₂O reduction. According to this, Bocking and Blyth (2018) assumed a very small pr in wet
553 soils, because N₂O may be trapped in the soil or completely reduced to N₂. This assumption may also
554 support results of the present study, where the average (N₂O+N₂) fluxes peaked at the medium water
555 saturation (particularly with GI soil) while D_{sim} decreased with increasing water saturations (Figure 4),
556 which may indicate an entrapment of (N₂O+N₂) in isolated soil pores (Clough et al., 2005; Harter et al.,
557 2016). However, N₂ release increased more strongly with time than the N₂O release resulting in
558 decreasing pr with time (Supplementary Material, Figure S5). The chance of N₂O to be released before it
559 is reduced to N₂ depends on the diffusion distance of dissolved (and gaseous) N₂O between its formation
560 sites and the atmosphere. Although diffusion pathways for O₂ and N₂O are similar just in opposite
561 direction, $ansvf$ and pr might be a good combination of proxies to predict N₂O emissions to capture
562 physical and microbial properties.



563 **4.2 How to substitute microscale information by bulk properties?**

564 The aims of this study were to find a minimum set of variables that explain the regulation of
565 microbial denitrification at microscopic scales in a simplified experimental setup and to explore in how
566 far this microscopic information can be substituted by readily available bulk properties that are feasible to
567 measure in a field campaign. The interplay of O₂ supply and oxygen demand resulted in CO₂ emissions
568 and CT-derived *ansvf* being the most important predictors for (N₂O+N₂) fluxes, while for N₂O fluxes *pr*
569 was also important (Figure 8, see Supplementary Material Figure S7). Simplified models with most
570 important predictors only (CO₂+ *ansvf* (+*pr*)) were sufficient to achieve similar explained variabilities
571 (71% and 83% for N₂O and (N₂O+N₂) fluxes, respectively) compared to the complex models. The
572 downside of using CO₂ and CT-derived *ansvf* as predictors for denitrification is that these proxies are
573 often unavailable and reasonable substitutions by easily available variables would be desirable.

574 The *ansvf* could have been replaced with alternative proxies for O₂ supply like D_{sim} , D_{emp} and ε_r ,
575 which would have led to a reduction in explained variability of (N₂O+N₂) fluxes to 64-76% and an even
576 larger drop for N₂O fluxes to 43-50% (Supplementary Material, Table S2, Figure S8). The substitution of
577 *ansvf* by D_{sim} would avoid the requirement for an ad-hoc definition of a critical pore distance threshold
578 but it is gained with the caveat of very time-consuming 3D simulations or laborious measurements.
579 Therefore, the substitution of *ansvf* with diffusivity estimated by empirical models (D_{emp}) seems more
580 viable. Diffusivity is mainly controlled by soil bulk density and water saturation (Balaine et al., 2013;
581 Klefoth et al., 2014). These empirical models predict diffusivity based on empirical relationships with
582 total porosity (Φ) and air-filled porosity (ε) (Deepagoda et al., 2011; Millington and Quirk, 1961;
583 Moldrup et al., 2000; Resurreccion et al., 2010; Deepagoda et al., 2019). As expected the discrepancy
584 between calculated D_{emp} and simulated D_{sim} was highest at water saturation >75% WFPS where
585 discontinuity due to packing procedure took full effect as described earlier (Supplementary Material,
586 Figure S8, Figure S4). The substitution of CT-derived *ansvf* by D_{emp} derived from empirical models
587 (Figure 8, Supplementary Material, Table S2) is perhaps unacceptable for a genuine understanding of
588 N₂O or (N₂O+N₂) emissions from individual samples since estimated diffusivity ignores the actual
589 tortuosity and continuity of the air-filled pore space. However, it may be a promising approach to
590 reasonably predict average N₂O or (N₂O+N₂) fluxes at natural conditions with readily available soil
591 characteristics (Figure 8, Figure S6). In this particular study, D_{sim} could even be replaced with the
592 theoretical air content (ε_r) adjusted during packing (together with CO₂(+*pr*)) without a reduction in
593 explained variability in N₂O and (N₂O+N₂) fluxes (Figure 8, Supplementary Material, Table S2), due to
594 the very strong log-linear relationship between the ε_r and D_{sim} (Figure 4e). However, totally neglecting



595 any proxy for O₂ supply, (i.e. CO₂ only to predict N₂O fluxes), was insufficient to predict N₂O fluxes
596 (Table S2).

597 A different strategy to estimate *ansvf* from bulk measurements is to switch from oxic to anoxic
598 incubation by replacing the carrier gas under otherwise constant conditions. The difference in (N₂O+N₂)
599 release between the two stages will be larger, the smaller the *ansvf* during oxic incubation. Details about
600 the calculation of this *ansvf_{cal}* can be found in the Supplementary Material. The *ansvf_{cal}* assumes that
601 actual denitrification is linearly related to *ansvf* and that the specific anoxic denitrification rate is
602 homogenous, i.e. would be identical at any location within the soil. Deviations from this assumption
603 could arise from heterogeneity in the distribution of substrates and microbial communities. However, the
604 actual soil volume where denitrification may occur, described by the distance to aerated pores, does not
605 only depend on O₂ diffusion, but also on respiration (O₂ consumption). Therefore, it could be expected,
606 that *ansvf* derived from X-ray CT imaging analysis compared to *ansvf_{cal}* was overestimated with RM soil
607 or underestimated with GI soil due to the differences in carbon sources and related O₂ consumption. The
608 average *ansvf_{cal}* was similar (0.20) to the *ansvf* (0.21) for RM soil (Supplementary Material, Table S3).
609 With GI soil, however, the *ansvf_{cal}* was larger (0.38) than the image-derived *ansvf* (0.13). This difference
610 may indeed result from an underestimation of *ansvf* due to the higher SOM content and respiration rates.
611 In future experiments it might be recommendable to integrate the O₂ consumption into *ansvf* estimation.
612 The appeal of this two-stage incubation is that it can be conducted with larger soil columns as there is no
613 size restriction as with the application of X-ray CT. Evidently, this two-stage incubation approach is not
614 feasible for field campaigns, for which we would recommend to resort to estimated diffusivities instead.

615 The use of CO₂ production as a proxy for O₂ demand to predict N₂O and (N₂O+N₂) release is limited
616 as it is not fully independent of denitrification, since anaerobic respiration contributes to total respiration.
617 Therefore, it is appealing to replace it with estimates of microbial activity based on empirical
618 relationships with temperature, SOM, clay and water content (Smith et al., 2003) as these properties are
619 routinely measured. When including the SOM measured before the experiment for the bulk soil (Table 1)
620 to explore N₂O or (N₂O+N₂) emissions, predictive power for (N₂O+N₂) decreased (57% compared to 83%
621 with CO₂ instead of SOM together with *ansvf*), just like it was reduced for predicting N₂O emissions
622 (60% compared to 71% with CO₂ instead of SOM together with *ansvf* and *pr*). The combination of
623 proxies for O₂ supply and demand, SOM and *D_{emp}* only, to predict N₂O and (N₂O+N₂) fluxes did not
624 reduce the explained variability too much beyond those of individual substitutions (50 and 58%,
625 respectively). An improvement might be achieved by accounting for different quality in SOM, e.g.
626 mineral-associated organic matter, fresh particulate organic matter, microbial pool; all of which will lead
627 to different mineralisation rates and hence propensity to run into local anoxia (Beauchamp et al., 1989;
628 Kuzyakov, 2015; Surey et al., 2020), due to the fact that SOM favours denitrification in several ways



629 (Ussiri and Lal, 2013; Beauchamp et al., 1989), i.e. by supplying energy, leading to consume O₂ via
630 respiration and supplying mineral N from mineralisation. Thus, in future studies the SOM content of bulk
631 soil or more involved empirical models that account for temperature and other independent variables
632 instead of values from the more laborious CO₂ measurement could be a promising variable to predict N₂O
633 emissions together with variables describing the soil structure.

634 **4.3 Future directions and implications for modeling**

635 In large-scale effective N-cycling models the *ansvf* is typically linked to the partial pressure of
636 oxygen in soil and conveys no explicit spatial information. In the long run these models like DNDC,
637 CoupModel, MicNiT (Li et al., 1992; Jansson and Karlberg, 2011; Blagodatsky et al., 2011) might benefit
638 tremendously from incorporating a spatially explicit *ansvf* as a state variable to predict denitrification.
639 The estimation of *ansvf* can be improved by taking O₂ consumption into account. Knowledge on spatial
640 distribution of respiration in combination with pore scale modeling would further improve *ansvf*
641 estimations and could be used to validate our approach with oxic/anoxic incubation. However, the
642 empirical functions to estimate this *ansvf* from readily available properties similar to empirical diffusivity
643 models have yet to be developed and validated against a whole suite of intact soil cores with different soil
644 types and vegetation for which oxic/anoxic incubation and X-ray CT analysis are carried out jointly.

645 Using intact instead of repacked soils in future experiments will represent more natural conditions,
646 e.g. larger tortuosity and thus lower diffusivity in undisturbed compared to sieved soil (Moldrup et al.,
647 2001). However, in undisturbed soils diffusivity and soil structure may also vary locally and as a
648 consequence of this varying O₂ supply and demand affect denitrification. Under field conditions this
649 impact on denitrification is additionally altered by temperature variations, atmospheric gas concentrations
650 and plant growth.

651 **Conclusions**

652 To our knowledge this is the first experimental setup combining X-ray CT derived imaging and flux
653 measurements of complete denitrification (i.e. N₂O and (N₂O+N₂) fluxes) to explore the microscopic
654 drivers of denitrification in repacked soil. We could show that changes in denitrification within different
655 saturations could be predicted well with the anaerobic soil volume fraction (*ansvf*) estimated from image-
656 derived soil structural properties. The differences in denitrification (i.e. N₂O and (N₂O+N₂) fluxes)
657 between two investigated soils were triggered by different respiration rates due to different SOM content.
658 A combination of CT-derived *ansvf* and CO₂ emission, as proxies for oxygen supply and demand,
659 respectively, is best in predicting (N₂O+N₂) emission (83% explained variability) across a large saturation



660 range and two different soils. The product ratio (pr), additionally to $ansvf$ and CO_2 emissions, was also an
661 important predictor for emissions of only the greenhouse gas N_2O (71% explained variability).

662 The $ansvf$ can also be replaced by simulated diffusivity (D_{sim}) (time consuming) or by diffusivity
663 from empirical models (D_{emp}) but not without losing predictive power. A replacement of CO_2 fluxes by
664 SOM also resulted in lower predictive power, but is recommended for large-scale applications since SOM
665 is an independent proxy for microbial activity. The full substitution of laborious predictors ($ansvf$, pr ,
666 CO_2) by readily available alternatives (SOM, D_{emp}) reduced the explained variability to 50 and 58% for
667 N_2O and (N_2O+N_2) fluxes, respectively.

668 The high explanatory power of image-derived $ansvf$ opens up new perspectives to make predictions
669 (e. g. by modelling approaches or in pedo-transfer functions) from independent measurements of soil
670 structure using new techniques (e.g. X-ray CT analysis) available today in combination with biotic
671 properties, e. g. quantity or quality of SOM. This paves the way for explicitly accounting for changes in
672 soil structure (e. g. tillage, plants) and climatic conditions (e. g. temperature, moisture) on denitrification.

673 *Data availability.* CT data and gas emission data are available from the authors on request.

674 *Author contribution.* H-JV, RW and SS designed the experiment. SS, BA and LR carried out the
675 experiment. G-MW developed the statistical analysis. SS and LR prepared the manuscript with
676 contributions from all co-authors.

677 *Competing interests.* The authors declare that they have no conflict of interest.

678 *Acknowledgments.* We thank Jürgen Böttcher from the Institute of Soil Science, Leibniz University in
679 Hannover, for measurements of soil materials used for incubation and Anette Giesemann and Martina
680 Heuer from Thünen-Institute for Climate-Smart Agriculture in Braunschweig, Germany, for isotopic
681 analysis. Our thanks go to Ines Backwinkel und Jan-Reent Köster from Thünen-Institute for Climate-
682 Smart Agriculture in Braunschweig, Germany, for conducting parallel incubations under oxic and anoxic
683 conditions. This study is funded by the Deutsche Forschungsgemeinschaft through the research unit
684 research unit DFG-FOR 2337: Denitrification in Agricultural Soils: Integrated Control and Modelling at
685 Various Scales (DASIM), grant umber 270261188.



686 **References**

- 687 Andersen, A. J., and Petersen, S. O.: Effects of C and N availability and soil-water potential interactions
688 on N₂O evolution and PLFA composition, *Soil Biol. Biochem.*, 41, 1726-1733,
689 <https://doi.org/10.1016/j.soilbio.2009.06.001>, 2009.
- 690
691 Aon, M. A., Sarena, D. E., Burgos, J. L., and Cortassa, S.: Interaction between gas exchange rates,
692 physical and microbiological properties in soils recently subjected to agriculture, *Soil Tillage Res.*, 60,
693 163-171, [https://doi.org/10.1016/S0167-1987\(01\)00191-X](https://doi.org/10.1016/S0167-1987(01)00191-X), 2001.
- 694
695 Arah, J. R. M., and Smith, K. A.: Steady-state denitrification in aggregated soil - A mathematical
696 approach, *Journal of Soil Science*, 40, 139-149, <https://doi.org/10.1111/j.1365-2389.1989.tb01262.x>,
697 1989.
- 698
699 Arah, J. R. M., and Vinten, A. J. A.: Simplified models of anoxia and denitrification in aggregated and
700 simple-structured soils, *European Journal of Soil Science*, 46, 507-517, [https://doi.org/10.1111/j.1365-
701 2389.1995.tb01347.x](https://doi.org/10.1111/j.1365-2389.1995.tb01347.x), 1995.
- 702
703 Balaine, N., Clough, T. J., Kelliher, F. M., and van Koten, C.: Soil aeration affects the degradation rate of
704 the nitrification inhibitor dicyandiamide, *Soil Research*, 53, 137-143, <https://doi.org/10.1071/SR14162>,
705 2015.
- 706
707 Balaine, N., Clough, T. J., Beare, M. H., Thomas, S. M., and Meenken, E. D.: Soil Gas Diffusivity
708 Controls N₂O and N₂ Emissions and their Ratio, *Soil Sc. Soc. Am. J.*, 80, 529-540,
709 <https://doi.org/10.2136/sssaj2015.09.0350>, 2016.
- 710
711 Beauchamp, E. G., Trevors, J. T., and Paul, J. W.: Carbon Sources for Bacterial Denitrification, in:
712 *Advances in Soil Science: Volume 10*, edited by: Stewart, B. A., Springer New York, New York, NY,
713 113-142, 1989.
- 714
715 Benjamini, Y., and Hochberg, Y.: Controlling the False Discovery Rate: A Practical and Powerful
716 Approach to Multiple Testing, *Journal of the Royal Statistical Society. Series B (Methodological)*, 57,
717 289-300, 1995.
- 718
719 Blagodatsky, S., Grote, R., Kiese, R., Werner, C., and Butterbach-Bahl, K.: Modelling of microbial
720 carbon and nitrogen turnover in soil with special emphasis on N-trace gases emission, *Plant and Soil*, 346,
721 297-330, <https://doi.org/10.1007/s11104-011-0821-z>, 2011.
- 722
723 Bocking, C. R., and Blyth, M. G.: Oxygen uptake and denitrification in soil aggregates, *Acta Mechanica*,
724 229, 595-612, <https://doi.org/10.1007/s00707-017-2042-x>, 2018.
- 725
726 Braker, G., and Conrad, R.: Diversity, structure, and size of N₂O-producing microbial communities in
727 soils-What matters for their functioning?, in: *Advances in Applied Microbiology*, Vol 75, edited by:
728 Laskin, A. I., Sariaslani, S., and Gadd, G. M., *Advances in Applied Microbiology*, 33-70, 2011.
- 729
730 Breiman, L.: Random Forests, *Machine Learning*, 45, 5-32, 10.1023/A:1010933404324, 2001.
- 731



- 732 Buchen, C., Lewicka-Szczebak, D., Fuß, R., Helfrich, M., Flessa, H., and Well, R.: Fluxes of N₂ and N₂O
733 and contributing processes in summer after grassland renewal and grassland conversion to maize cropping
734 on a Plagic Anthrosol and a Histic Gleysol, *Soil Biol. Biochem.*, 101, 6-19,
735 <http://dx.doi.org/10.1016/j.soilbio.2016.06.028>, 2016.
- 736
737 Butterbach-Bahl, K., Baggs, E. M., Dannenmann, M., Kiese, R., and Zechmeister-Boltenstern, S.: Nitrous
738 oxide emissions from soils: how well do we understand the processes and their controls?, *Philosophical*
739 *Transactions of the Royal Society B: Biological Sciences*, 368, <https://doi.org/10.1098/rstb.2013.0122>,
740 2013.
- 741
742 Cabello, P., Roldán, M. D., and Moreno-Vivián, C.: Nitrate reduction and the nitrogen cycle in archaea,
743 *Microbiology*, 150, 3527-3546, doi:10.1099/mic.0.27303-0, 2004.
- 744
745 Canty, A., and Ripley, B.: boot: Bootstrap R (S-Plus) Functions . R package version 1.3-24, 2019.
- 746
747 Clough, T. J., Sherlock, R. R., and Rolston, D. E.: A Review of the Movement and Fate of N₂O in the
748 Subsoil, *Nutrient Cycling in Agroecosystems*, 72, 3-11, <https://doi.org/10.1007/s10705-004-7349-z>, 2005.
- 749
750 Davidson, E. A., Verchot, L. V., Cattânio, J. H., Ackerman, I. L., and Carvalho, J. E. M.: Effects of Soil
751 Water Content on Soil Respiration in Forests and Cattle Pastures of Eastern Amazonia, *Biogeochemistry*,
752 48, 53-69, <https://doi.org/10.1023/A:1006204113917>, 2000.
- 753
754 Davison, A. C., and Hinkley, D. V.: Bootstrap Methods and their Application, Cambridge Series in
755 Statistical and Probabilistic Mathematics, Cambridge University Press, Cambridge, 1997.
- 756
757 Deepagoda, T., Moldrup, P., Schjonning, P., de Jonge, L. W., Kawamoto, K., and Komatsu, T.: Density-
758 Corrected Models for Gas Diffusivity and Air Permeability in Unsaturated Soil, *Vadose Zone J.*, 10, 226-
759 238, <https://doi.org/10.2136/vzj2009.0137>, 2011.
- 760
761 Deepagoda, T., Jayarathne, J., Clough, T. J., Thomas, S., and Elberling, B.: Soil-Gas Diffusivity and Soil-
762 Moisture effects on N₂O Emissions from Intact Pasture Soils, *Soil Sc. Soc. Am. J.*, 83, 1032-1043,
763 10.2136/sssaj2018.10.0405, 2019.
- 764
765 Ebrahimi, A., and Or, D.: Dynamics of soil biogeochemical gas emissions shaped by remolded aggregate
766 sizes and carbon configurations under hydration cycles, *Glob. Change Biol.*, 24, e378-e392,
767 <https://doi.org/10.1111/gcb.13938>, 2018.
- 768
769 Efron, B.: Better Bootstrap Confidence Intervals, *Journal of the American Statistical Association*, 82,
770 171-185, 10.2307/2289144, 1987.
- 771
772 Elberling, B., Askaer, L., Jørgensen, C. J., Joensen, H. P., Kühl, M., Glud, R. N., and Lauritsen, F. R.:
773 Linking Soil O₂, CO₂, and CH₄ Concentrations in a Wetland Soil: Implications for CO₂ and CH₄ Fluxes,
774 *Environmental Science & Technology*, 45, 3393-3399, <https://doi.org/10.1021/es103540k>, 2011.
- 775
776 Greenwood, D. J.: The effect of oxygen concentration on the decomposition of organic materials in soil,
777 *Plant and Soil*, 14, 360-376, <https://doi.org/10.1007/BF01666294>, 1961.
- 778



- 779 Groffman, P. M., and Tiedje, J. M.: Denitrification hysteresis during wetting and drying cycles in soil,
780 *Soil Sci Soc Am J*, 52, <https://doi.org/10.2136/sssaj1988.03615995005200060022x>, 1988.
- 781
- 782 Groffman, P. M., Altabet, M. A., Bohlke, J. K., Butterbach-Bahl, K., David, M. B., Firestone, M. K.,
783 Giblin, A. E., Kana, T. M., Nielsen, L. P., and Voytek, M. A.: Methods for measuring denitrification:
784 Diverse approaches to a difficult problem, *Ecological Applications*, 16, 2091-2122,
785 [https://doi.org/10.1890/1051-0761\(2006\)016\[2091:mfmdda\]2.0.co;2](https://doi.org/10.1890/1051-0761(2006)016[2091:mfmdda]2.0.co;2), 2006.
- 786
- 787 Harter, J., Guzman-Bustamante, I., Kuehfuss, S., Ruser, R., Well, R., Spott, O., Kappler, A., and Behrens,
788 S.: Gas entrapment and microbial N₂O reduction reduce N₂O emissions from a biochar-amended sandy
789 clay loam soil, *Scientific Reports*, 6, 39574, 10.1038/srep39574
790 <http://www.nature.com/articles/srep39574#supplementary-information>, 2016.
- 791
- 792 Hayatsu, M., Tago, K., and Saito, M.: Various players in the nitrogen cycle: Diversity and functions of
793 the microorganisms involved in nitrification and denitrification, *Soil Science & Plant Nutrition*, 54, 33-
794 45, <https://doi.org/10.1111/j.1747-0765.2007.00195.x>, 2008.
- 795
- 796 Herbst, M., Tappe, W., Kummer, S., and Vereecken, H.: The impact of sieving on heterotrophic
797 respiration response to water content in loamy and sandy topsoils, *Geoderma*, 272, 73-82,
798 <https://doi.org/10.1016/j.geoderma.2016.03.002>, 2016.
- 799
- 800 Højberg, O., Revsbech, N. P., and Tiedje, J. M.: Denitrification in Soil Aggregates Analyzed with
801 Microsensors for Nitrous Oxide and Oxygen, *Soil Sc. Soc. Am. J.*, 58, 1691-1698,
802 doi:10.2136/sssaj1994.03615995005800060016x, 1994.
- 803
- 804 Iassonov, P., and Tuller, M.: Application of segmentation for correction of intensity bias in X-ray
805 computed tomography images, *Vadose Zone Journal*, 9, 187-191, 2010.
- 806
- 807 Jäger, H. J., Schmidt, S. W., Kammann, C., Grunhage, L., Muller, C., and Hanewald, K.: The University
808 of Giessen Free-Air Carbon Dioxide Enrichment study: Description of the experimental site and of a new
809 enrichment system, *J. Appl. Bot.-Angew. Bot.*, 77, 117-127, 2003.
- 810
- 811 Jansson, P.-E., and Karlberg, L.: COUP Manual: Coupled heat and mass transfer model for soil-plant-
812 atmosphere systems, <https://www.coupmodel.com/documentation>, 2011.
- 813
- 814 John, B., Yamashita, T., Ludwig, B., and Flessa, H.: Storage of organic carbon in aggregate and density
815 fractions of silty soils under different types of land use, *Geoderma*, 128, 63-79,
816 <https://doi.org/10.1016/j.geoderma.2004.12.013>, 2005.
- 817
- 818 Jones, C. M., Stres, B., Rosenquist, M., and Hallin, S.: Phylogenetic analysis of nitrite, nitric oxide, and
819 nitrous oxide respiratory enzymes reveal a complex evolutionary history for denitrification, *Mol. Biol.*
820 *Evol.*, 25, 1955-1966, <https://doi.org/10.1093/molbev/msn146>, 2008.
- 821
- 822 Keiluweit, M., Nico, P. S., Kleber, M., and Fendorf, S.: Are oxygen limitations under recognized
823 regulators of organic carbon turnover in upland soils?, *Biogeochemistry*, 127, 157-171,
824 <https://doi.org/10.1007/s10533-015-0180-6>, 2016.
- 825



- 826 Keiluweit, M., Gee, K., Denney, A., and Fendorf, S.: Anoxic microsites in upland soils dominantly
827 controlled by clay content, *Soil Biol. Biochem.*, 118, 42-50, <https://doi.org/10.1016/j.soilbio.2017.12.002>,
828 2018.
- 829
830 Knowles, R.: Denitrification, *Microbiol. Rev.*, 46, 43-70, 1982.
- 831
832 Kravchenko, A. N., Guber, A. K., Quigley, M. Y., Koestel, J., Gandhi, H., and Ostrom, N. E.: X-ray
833 computed tomography to predict soil N₂O production via bacterial denitrification and N₂O emission in
834 contrasting bioenergy cropping systems, *GCB Bioenergy*, 10, 894-909,
835 <https://doi.org/10.1111/gcbb.12552>, 2018.
- 836
837 Kravchenko, A. N., Guber, A. K., Razavi, B. S., Koestel, J., Quigley, M. Y., Robertson, G. P., and
838 Kuzyakov, Y.: Microbial spatial footprint as a driver of soil carbon stabilization, *Nature Communications*,
839 10, 3121, <https://doi.org/10.1038/s41467-019-11057-4>, 2019.
- 840
841 Kremen, A., Bear, J., Shavit, U., and Shaviv, A.: Model demonstrating the potential for coupled
842 nitrification denitrification in soil aggregates, *Environmental Science & Technology*, 39, 4180-4188,
843 <https://doi.org/10.1021/es048304z>, 2005.
- 844
845 Kuzyakov, Y.: Microbial hotspots and hot moments in soil: Concept & review, *Soil Biol. Biochem.*, v.
846 83, pp. 184-199-2015 v.2083, <https://doi.org/10.1016/j.soilbio.2015.01.025>, 2015.
- 847
848 Legland, D., Arganda-Carreras, I., and Andrey, P.: MorphoLibJ: integrated library and plugins for
849 mathematical morphology with ImageJ, *Bioinformatics*, 32, 3532-3534, 2016.
- 850
851 Lewicka-Szczebak, D., Well, R., Giesemann, A., Rohe, L., and Wolf, U.: An enhanced technique for
852 automated determination of ¹⁵N signatures of N₂, (N₂+N₂O) and N₂O in gas samples, *Rapid Commun.*
853 *Mass Spec.*, 27, 1548-1558, <https://doi.org/10.1002/rcm.6605>, 2013.
- 854
855 Li, C. S., Frolking, S., and Frolking, T. A.: A model of nitrous oxide evolution from soil driven by rainfall
856 events: 1. Model structure and sensitivity, *J. Geophys. Res.-Atmos.*, 97, 9759-9776,
857 <https://doi.org/10.1029/92jd00509>, 1992.
- 858
859 Millington, R., and Quirk, J. P.: Permeability of porous solids, *Transactions of the Faraday Society*, 57,
860 1200-&, <https://doi.org/10.1039/tf9615701200>, 1961.
- 861
862 Millington, R. J., and Quirk, J. M.: Transport in porous media, in: F.A. Van Beren et. al (ed.), *Trans. Int.*
863 *Congr. Soil Sci.*, 7th, Madison, WI. 14–21 Aug, Elsevier, Amsterdam, 97–106, 1960.
- 864
865 Moldrup, P., Olesen, T., Yamaguchi, T., Schjønning, P., and Rolston, D. E.: Modeling diffusion and
866 reaction in soils: IX. The Buckingham-Burdine-Campbell equation for gas diffusivity in undisturbed soil,
867 *Soil Science*, 164, 542-551, 1999.
- 868
869 Moldrup, P., Olesen, T., Gamst, J., Schjønning, P., Yamaguchi, T., and Rolston, D. E.: Predicting the gas
870 diffusion coefficient in repacked soil: Water-induced linear reduction model, *Soil Sc. Soc. Am. J.*, 64,
871 1588-1594, <https://doi.org/10.2136/sssaj2000.6451588x>, 2000.
- 872



- 873 Moldrup, P., Olesen, T., Komatsu, T., Schjønning, P., and Rolston, D. E.: Tortuosity, Diffusivity, and
874 Permeability in the Soil Liquid and Gaseous Phases, *Soil Sc. Soc. Am. J.*, 65, 613-623,
875 doi:10.2136/sssaj2001.653613x, 2001.
- 876
877 Morley, N. J., Richardson, D. J., and Baggs, E. M.: Substrate Induced Denitrification over or under
878 Estimates Shifts in Soil N₂/N₂O Ratios, *Plos One*, 9, <https://doi.org/10.1371/journal.pone.0108144>,
879 2014.
- 880
881 Moyano, F. E., Vasilyeva, N., Bouckaert, L., Cook, F., Craine, J., Curiel Yuste, J., Don, A., Epron, D.,
882 Formanek, P., Franzluebbers, A., Ilstedt, U., Kätterer, T., Orchard, V., Reichstein, M., Rey, A., Ruamps,
883 L., Subke, J. A., Thomsen, I. K., and Chenu, C.: The moisture response of soil heterotrophic respiration:
884 interaction with soil properties, *Biogeosciences*, 9, 1173-1182, <https://doi.org/10.5194/bg-9-1173-2012>,
885 2012.
- 886
887 Müller, C., and Clough, T. J.: Advances in understanding nitrogen flows and transformations: gaps and
888 research pathways, *J. Agric. Sci.*, 152, S34-S44, <https://doi.org/10.1017/s0021859613000610>, 2014.
- 889
890 Nengsih, T. A., Bertrand, F., Maumy-Bertrand, M., and Meyer, N.: Determining the number of
891 components in PLS regression on incomplete data set, *Stat. Appl. Genet. Mol. Biol.*, 18, 28,
892 10.1515/sagmb-2018-0059, 2019.
- 893
894 Otsu, N.: A threshold selection method from gray-level histograms, *Automatica*, 11, 23-27, 1975.
- 895
896 Philippot, L., Hallin, S., and Schloter, M.: Ecology of Denitrifying Prokaryotes in Agricultural Soil, in:
897 *Advances in Agronomy*, edited by: Donald, L. S., Academic Press, 249-305, 2007.
- 898
899 Porre, R. J., van Groenigen, J. W., De Deyn, G. B., de Goede, R. G. M., and Lubbers, I. M.: Exploring the
900 relationship between soil mesofauna, soil structure and N₂O emissions, *Soil Biol. Biochem.*, 96, 55-64,
901 <https://doi.org/10.1016/j.soilbio.2016.01.018>, 2016.
- 902
903 R Core Team: R: A language and environment for statistical computing. R Foundation for Statistical
904 Computing, Vienna, Austria. URL <https://www.R-project.org/>, 2018.
- 905
906 Rabot, E., Lacoste, M., Henault, C., and Cousin, I.: Using X-ray Computed Tomography to Describe the
907 Dynamics of Nitrous Oxide Emissions during Soil Drying, *Vadose Zone J.*, 14, 10,
908 <https://doi.org/10.2136/vzj2014.12.0177>, 2015.
- 909
910 Reichstein, M., and Beer, C.: Soil respiration across scales: The importance of a model-data integration
911 framework for data interpretation, *Journal of Plant Nutrition and Soil Science*, 171, 344-354,
912 <https://doi.org/10.1002/jpln.200700075>, 2008.
- 913
914 Resurreccion, A. C., Moldrup, P., Kawamoto, K., Hamamoto, S., Rolston, D. E., and Komatsu, T.:
915 Hierarchical, Bimodal Model for Gas Diffusivity in Aggregated, Unsaturated Soils, *Soil Sc. Soc. Am. J.*,
916 74, 481-491, <https://doi.org/10.2136/sssaj2009.0055>, 2010.
- 917
918 Ryan, M. G., and Law, B. E.: Interpreting, measuring, and modeling soil respiration, *Biogeochemistry*,
919 73, 3-27, <https://doi.org/10.1007/s10533-004-5167-7>, 2005.



- 920
921 Schindelin, J., Arganda-Carreras, I., Frise, E., Kaynig, V., Longair, M., Pietzsch, T., Preibisch, S.,
922 Rueden, C., Saalfeld, S., and Schmid, B.: Fiji: an open-source platform for biological-image analysis,
923 Nature methods, 9, 676-682, 2012.
- 924
925 Schlüter, S., Sheppard, A., Brown, K., and Wildenschild, D.: Image processing of multiphase images
926 obtained via X-ray microtomography: A review, Water Resources Research, 50, 3615-3639,
927 <https://doi.org/10.1002/2014wr015256>, 2014.
- 928
929 Schlüter, S., Leuther, F., Vogler, S., and Vogel, H.-J.: X-ray microtomography analysis of soil structure
930 deformation caused by centrifugation, Solid Earth, 7, 129-140, 2016.
- 931
932 Schlüter, S., Zawallich, J., Vogel, H. J., and Dörsch, P.: Physical constraints for respiration in microbial
933 hotspots in soil and their importance for denitrification, Biogeosciences Discuss., 2019, 1-31,
934 <https://doi.org/10.5194/bg-2019-2>, 2019.
- 935
936 Senbayram, M., Chen, R., Budai, A., Bakken, L., and Dittert, K.: N₂O emission and the N₂O/(N₂O+N₂)
937 product ratio of denitrification as controlled by available carbon substrates and nitrate concentrations,
938 Agriculture, Ecosystems & Environment, 147, 4-12, <https://doi.org/10.1016/j.agee.2011.06.022>, 2012.
- 939
940 Sexstone, A. J., Revsbech, N. P., Parkin, T. B., and Tiedje, J. M.: Direct measurement of oxygen profiles
941 and denitrification rates in soil aggregates, Soil Sc. Soc. Am. J., 49, 645-651, 1985.
- 942
943 Shoun, H., Kim, D.-H., Uchiyama, H., and Sugiyama, J.: Denitrification by fungi, FEMS Microbiol. Lett.,
944 94, 277-281, 1992.
- 945
946 Smith, K. A., Ball, T., Conen, F., Dobbie, K. E., Massheder, J., and Rey, A.: Exchange of greenhouse
947 gases between soil and atmosphere: interactions of soil physical factors and biological processes,
948 European Journal of Soil Science, 54, 779-791, <https://doi.org/10.1046/j.1351-0754.2003.0567.x>, 2003.
- 949
950 Spott, O., Russow, R., Apelt, B., and Stange, C. F.: A ¹⁵N-aided artificial atmosphere gas flow technique
951 for online determination of soil N₂ release using the zeolite Köstrolith SX6®, Rapid Commun. Mass
952 Spec., 20, 3267-3274, <https://doi.org/10.1002/rcm.2722>, 2006.
- 953
954 Surey, R., Lippold, E., Heilek, S., Sauheitl, L., Henjes, S., Horn, M. A., Mueller, C. W., Merbach, I.,
955 Kaiser, K., Böttcher, J., and Mikutta, R.: Differences in labile soil organic matter explain potential
956 denitrification and denitrifying communities in a long-term fertilization experiment, Appl. Soil. Ecol.,
957 153, 103630, <https://doi.org/10.1016/j.apsoil.2020.103630>, 2020.
- 958
959 Syakila, A., and Kroeze, C.: The global nitrous oxide budget revisited, Greenhouse Gas Measurement and
960 Management, 1, 17-26, <https://doi.org/10.3763/ghgmm.2010.0007>, 2011.
- 961
962 Thompson, R. L., Lassaletta, L., Patra, P. K., Wilson, C., Wells, K. C., Gressent, A., Koffi, E. N.,
963 Chipperfield, M. P., Winiwarter, W., Davidson, E. A., Tian, H., and Canadell, J. G.: Acceleration of
964 global N₂O emissions seen from two decades of atmospheric inversion, Nature Climate Change, 9, 993-
965 998, <https://doi.org/10.1038/s41558-019-0613-7>, 2019.
- 966



- 967 Tiedje, J. M.: Ecology of denitrification and dissimilatory nitrate reduction to ammonium, in:
968 Environmental Microbiology of Anaerobes, edited by: Zehnder, A. J. B., John Wiley and Sons, N.Y.,
969 179-244, 1988.
- 970
971 Ussiri, D., and Lal, R.: Soil Emission of Nitrous Oxide and its Mitigation, Springer, 2013.
- 972
973 van Cleemput, O.: Subsoils: chemo- and biological denitrification, N₂O and N₂ emissions, Nutrient
974 Cycling in Agroecosystems, 52, 187-194, <https://doi.org/10.1023/a:1009728125678>, 1998.
- 975
976 Wickham, H.: ggplot2: Elegant Graphics for Data Analysis. Springer-Verlag New York, 2016.
- 977
978 Wiegmann, A., and Bube, K. P.: The explicit-jump immersed interface method: Finite difference methods
979 for PDEs with piecewise smooth solutions, SIAM J. Numer. Anal., 37, 827-862,
980 <https://doi.org/10.1137/S0036142997328664>, 2000.
- 981
982 Wiegmann, A., and Zemitis, A.: EJ-HEAT: A fast explicit jump harmonic averaging solver for the
983 effective heat conductivity of composite materials, Berichte des Fraunhofer ITWM, 94, 2006.
- 984
985 Wolodzko, T.: kernelboot: Smoothed Bootstrap and Random Generation from Kernel Densities, 2020.
- 986
987 Zumft, W. G.: Cell biology and molecular basis of denitrification, Microbiology and Molecular Biology
988 Reviews, 61, 533-616, 1997.
- 989
990